

# Characterization by Mercury Porosimetry of Nonwoven Fiber Media with Deformation

Gregory C. Rutledge, Joseph L. Lowery, Chia-Ling Pai

Department of Chemical Engineering and Institute for Soldier Nanotechnologies  
Massachusetts Institute of Technology, Cambridge, Massachusetts UNITED STATES

Correspondence to:

Gregory C. Rutledge email: [Rutledge@mit.edu](mailto:Rutledge@mit.edu)

## ABSTRACT

The porosity and pore diameter distribution are important characteristics of nonwoven fiber media. With the advent of electrospinning, the production of mats of nonwoven fibrous materials with fiber diameters in the 0.1-10  $\mu\text{m}$  range has become more prevalent. The large compliance of these mats makes them susceptible to mechanical deformation under the pressures attained in a typical mercury porosimetry experiment. We report a theoretical analysis of the liquid volume measured during liquid intrusion porosimetry in the presence of deformation of such mats by one of two modes: buckling of the pores or elastic compression of the mat. For electrospun mats of poly( $\epsilon$ -caprolactone) with average fiber diameters ranging from 2.49 to 18.0  $\mu\text{m}$ , we find that buckling is the more relevant mode of deformation, and that it can alter significantly the determination of pore diameter distributions measured by mercury porosimetry.

Keywords: porosimetry; pore size distribution; electrospinning; nanofiber; nonwoven; buckling; elasticity; deformation

## INTRODUCTION

Over the past ten years, electrospun nonwoven materials have become popular for a variety of applications, due primarily to the small fiber diameters involved and the correspondingly high specific surface area achievable, as well as the remarkable ease with which such materials are formed from a broad range of synthetic and natural polymers. The application that has received probably the greatest attention is tissue engineering. For applications such as this, not only the fiber size but also the porosity of the nonwoven material and its

distribution among pores of various sizes are important. The fiber size distribution of these materials is readily quantified by measurements taken from scanning electron micrographs (SEM). The pore size distribution or pore volume distribution, on the other hand, are somewhat more difficult to characterize accurately, and are less frequently reported despite their obvious importance. Reasons for this have to do with the irregular shape and copious interconnectivity of the void spaces within a fibrous nonwoven material, as well as the relative ease with which these materials are deformed. The purpose of this report is to understand the origin and magnitude of the corrections associated with deformation of such porous materials at high pressure, in order to make the most accurate estimation of pore volume (or size) distribution from liquid intrusion porosimetry data. The analysis is general, however; it is not limited to electrospun mats or even to fibrous materials.

To date, several methods have been reported to characterize the porosity of electrospun nonwoven membranes [1-5]. The first of these is capillary flow porometry, which is based on the difference in flow rates of a gas through the dry membrane and through the membrane wetted with a low surface energy fluid; it is useful for characterizing the mean flow pore diameter, which is the size of the smallest constriction in the pores through which 50% of the gas flows when the membrane is dry [2]. While useful for transport applications, this method does not quantify the distribution of pore volume within the membrane. For this purpose, mercury intrusion porosimetry and liquid extrusion porosimetry are used. Mercury intrusion relies on the measurement of the volume of a non-wetting liquid, in this case

mercury, intruded into the pores of the membrane as pressure is increased, while liquid extrusion relies on the measurement of the volume of a wetting liquid that is extruded from the pores of the membrane as pressure is increased. Whether a liquid is wetting or non-wetting depends on its contact angle,  $\theta$ , with the material of the membrane. The pressure  $P$  at which the wetting liquid is extruded from, or the non-wetting liquid intruded into, the pores is determined by the Washburn equation:

$$P_i = \alpha/D \quad (1)$$

where  $D$  is the diameter of the pore and  $\alpha = \pm 4\gamma \cos\theta$ .  $\gamma$  is the surface energy of the liquid. '+' corresponds to liquid extrusion, where  $\cos\theta > 0$ , and '-' corresponds to liquid intrusion, where  $\cos\theta < 0$ . Mercury is typically the liquid of choice for intrusion porosimetry because it exhibits a very high contact angle of 130-140° with most materials. For reasons of symmetry discussed below, mercury intrusion porosimetry offers better opportunity to measure accurately the total pore volume of the membrane than does liquid extrusion porosimetry, but potentially suffers from inaccuracies due to the high pressures that are often required to intrude mercury into the smallest pores of the membrane. This is especially true for very compliant materials like electrospun nonwoven fiber mats, where both the fibers and the pores are one to two orders of magnitude smaller in diameter than those in conventional fiber media. Similar problems have been recognized in the study of xerogels and aerogels, where deformation of the sample may distort or preclude altogether the measurement of pore size distributions [6-8].

*Fig 1a* is a simplified, two-dimensional representation of a porous material that serves to illustrate three types of pores that may occur in a fibrous membrane wherein the fibers are oriented predominantly within the plane of the membrane. Each pore has structure, in that the diameter of the pore may vary along its length; the length scale of such variation is characterized by the distance " $l$ ". In an electrospun nonwoven mat,  $l$  is probably on the order of one to several times the average diameter of the fibers. Thus, each pore can be approximated by a collection of pore sections that differ in diameter. For nonwoven membranes where pores are multiply connected, it is sufficient to consider only the sequence of sections of largest diameter that provides access to the volume of a given pore section, since this determines the pressure at which liquid is intruded into or extruded from that section. In this

way, a complicated, multiply-connected pore network can be decomposed into a set of "simple pores" like those illustrated in *Fig 1a*.

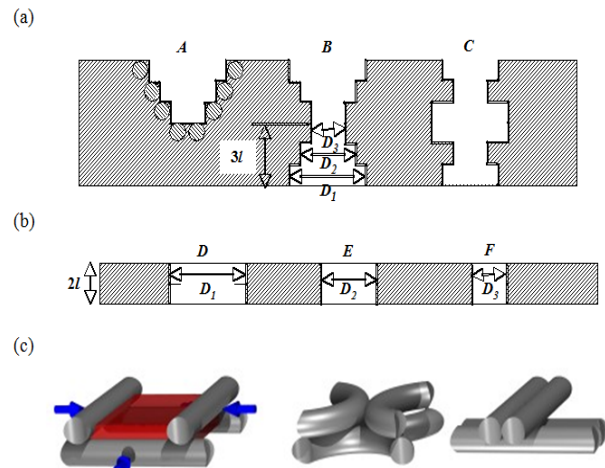


FIGURE 1. Schematic diagram of pore geometry in a membrane. (a) blind pore (A), through pore with single constriction (B), and through pore with two constrictions (C). The circles surrounding pore A represent cross-sections of fibers and illustrate schematically in 2D how such a pore might be defined in a nonwoven fiber membrane. (b) Equivalent pore size distribution corresponding to (B), as measured by liquid intrusion porosimetry, broken down into pore sections. (c) Illustration of two mechanisms by which buckling of a pore section, defined in this simple example by only four fibers, might occur. The leftmost image is the pore section prior to buckling; the liquid pressure on the section is indicated by blue arrows, while the volume of the pore section is shown in red. Buckling can occur through bending deformation of the fibers that define the circumference of the pore section (center image) or through sliding of the fibers relative to one another (rightmost image); either mechanism leads to expansion of the liquid volume exterior to the pore section, at the expense of the volume of the pore section itself. Elastic compression would appear similar structurally to buckling, with the difference that the entire unfilled portion of the mat deforms homogeneously, affinely and in either 2 or 3 dimensions

Pore A is a "blind" pore that does not provide a contiguous pathway from one side of the membrane to the other. Such pores are measured by liquid intrusion porosimetry but not by liquid extrusion [1], but in any case are expected to be of little consequence in nonwoven fiber media. Pores B and C are examples of "through" pores; B has a single constriction, while C is representative of pores with two or more constrictions, which results in the possibility of internal voids within the membrane that are accessible only via constrictions or "gateways". By virtue of the fact that liquid intrusion proceeds from both sides of the membrane as pressure is increased, the liquid volume is measured for each segment of pore B as the pressure rises to a level sufficient to drive the liquid deeper into the pore.

Liquid extrusion porosimetry, on the other hand, relies on application of gas pressure to only one side of the wetted membrane, so that the liquid is extruded from the other side. As a result, liquid volume is measured for each segment on the upstream side of the pore constriction as the pressure rises to a level sufficient to displace the liquid; however, once the pressure sufficient to extrude liquid from the smallest constriction (diameter  $D_3$  in *Fig 1a*) is reached, the downstream side of the pore is spontaneously emptied, thus leading to overestimation of the volume associated with pore segments of diameter  $D_3$ . Thus, liquid intrusion porosimetry is expected to provide a more accurate measure of the pore volume for both pore types A and B.

Neither method measures correctly the volume associated with internal voids such as that illustrated by pore C; as the pressure rises to a level sufficient to intrude (or extrude) liquid from the smallest constriction ( $D_3$ ), the remaining cavity (diameter  $D_1$ ) fills spontaneously, again leading to overestimation of the volume associated with segments of diameter  $D_3$ . This type of error appears to be intrinsic to liquid intrusion (extrusion) methods, and has been called the “ink bottle effect” [9]. The presence of such pores with internal voids can be estimated from the hysteresis in the liquid volume recovered as the system is depressurized. *Fig 1b* illustrates the decomposition of a pore of type B into multiple pore sections (D,E,F) of uniform diameter and length  $2l$ , as illustrated in *Fig 1b*; pores of Type A can be treated similarly. The deformation of membranes such as that shown in *Fig 1b* is dealt with in the next section.

## THEORY

For purposes of characterizing its mechanical response to an applied pressure, the membrane is treated as a homogeneous, isotropic material with an effective Young’s modulus  $E$  and Poisson’s ratio  $\nu$ . The bulk modulus of such a material is  $K = E/3(1-2\nu)$ . Under compression, the membrane may deform by two mechanisms: (i) pores buckle under the applied pressure, or (ii) the entire membrane deforms elastically. We consider both mechanisms here.

### The Buckling-Intrusion Transition

In this case, we assume that the pores in *Fig 1b* may be approximated by thin cylindrical shells of thickness  $t$  and diameter  $D$ . Such shells may buckle

under axial or radial loading. Here we consider the case of uniform external pressure (radial loading) that leads to radial collapse of the cylinder. *Fig 1c* illustrates what such a radial collapse might look like in a fibrous material, for a particularly simplified pore section in which the “cylinder” is defined by only four fibers. Whether the collapse occurs through bending of the fibers or the sliding of fibers relative to one another is not essential for this analysis, since both are reflected in the effective Young’s modulus  $E$  for the membrane; in reality, some combination of the two is likely. For simplicity, we consider here the limit of  $l/D \gg 1$ , although the equation for radial buckling of a ring, applicable for  $l/D \ll 1$ , differs only by a constant prefactor [10]. The buckling pressure is given by [11]:

$$P_b = \frac{E}{4} \left( \frac{2t}{D} \right)^3 \quad (2)$$

The buckling pressure  $P_b$  scales as the -3 power of pore diameter according to Eq. (2), whereas the intrusion pressure  $P_i$  scales as the -1 power of pore diameter according to Eq. (1), so there exists a critical pressure  $P_c$  below which pores tend to buckle rather than fill by liquid intrusion. Equating  $P_i$  and  $P_b$ , we can solve for the critical diameter  $D_c$  and pressure at which this buckling-intrusion transition occurs:

$$D_c = (2Et^3/\alpha)^{1/2} \quad (3)$$

$$P_c = (\alpha^3/2Et^3)^{1/2} \quad (4)$$

Significantly, if buckling occurs due to loads transmitted throughout membrane, it may occur anywhere within the membrane and is not subject to the type of error associated with intrusion through a constriction, as illustrated by pore C in *Fig 1a*. Regardless whether the pore buckles or fills by intrusion, the volume of liquid measured by the intrusion porosimetry experiment is assumed to be the same; for purposes of illustration, we assume that the volume is cylindrical, in accord with *Fig 1a*, i.e.  $V = \pi D^2 l/4$ , but other forms for  $V(D)$  are also conceivable. Thus, for a single pore, one can write the volume of liquid measured during the intrusion experiment as a function of pressure as follows:

$$v(P) = \int_0^P V \delta(P' - P^*) dP' \quad (5)$$

where  $P^*$  is the buckling pressure for  $P < P_c$ , or the intrusion pressure for  $P \geq P_c$ . Eq. (5) can be generalized for a distribution of pores,  $\rho(D)$ , defined such that:

$$\int_0^{\infty} \rho(D) dD = 1 \quad (6)$$

Given a distribution of pore sizes,  $v(P)$  is the cumulative volume of liquid measured as a function of pressure during the porosimetry experiment:

$$v(P) = \int_0^P \rho(D) V(D) \left[ -\frac{dD}{dP'} \right] dP' \quad (7)$$

where

$$\left[ -\frac{dD}{dP} \right] = \begin{cases} \frac{2t}{3P} \left( \frac{E}{4P} \right)^{1/3} = \frac{D}{3P} & \text{for } P < P_c \\ & \text{(buckling)} \\ \frac{\alpha}{P^2} = \frac{D}{P} & \text{for } P \geq P_c \\ & \text{(intrusion)} \end{cases} \quad (8)$$

The log differential volume measured as a function of  $P$  can be written:

$$\frac{dv(P)}{d \log P} = \rho(D) V(D) \left[ -\frac{dD}{dP} \right] P \quad (9)$$

Alternatively, the log differential volume can be expressed in terms of the *equivalent capillary diameter*  $D_{eq}$ , where care in nomenclature is taken to distinguish between the true pore diameter measured by buckling at a pressure  $P$  and the equivalent diameter that would be inferred assuming the pore filled by intrusion at this same pressure.

$$\frac{dv(D_{eq})}{d \log D_{eq}} = \rho(D_{eq}) V(D_{eq}) D_{eq} = \frac{dv(P)}{d \log P} \quad (10)$$

Within the limitations of applicability of Eq. (1) for intrusion and Eq. (2) for buckling, the resulting pore size distribution can be measured over the entire range of pressure. Other modes of buckling may also be considered in lieu of Eq. (2), depending on the nature of the porous medium. In their studies of xerogels and aerogels, Pirard et al [7] proposed a model based on Euler buckling of a cubic cage-like structure such as that used to describe the elastic properties of open cell foams [12]. In that model,  $P = n\pi^2 EI / D^4$  and  $I = \pi t^4 / 64$  (using the current nomenclature). Similar equations can also be written

for axial buckling of a cylindrical shell (or buckling of a spherical shell [11]):

$$\left( P = 2E(3 - 3\nu^2)^{-1/2} (2t / D)^2 \right)$$

Each of these is straightforward to implement within the current analysis, starting with the replacement of Eq. (2). Each leads to a different dependence of pore diameter on pressure in the buckling regime. In the absence of an independent method like nitrogen absorption [7] to determine this relationship for pores on the order of microns or larger, we adopt here the radial cylindrical buckling model as being most representative of the geometry of electrospun nonwovens, with the understanding that it is illustrative of the approach; we defer further discrimination between buckling models to a subsequent study.

### Elastic compression-Intrusion

In this case, we assume that as the liquid pressure is increased, the membrane deforms elastically with bulk modulus  $K$ , but that the volume lost occurs solely through reduction in volume of the unfilled pores in the membrane. A deformed pore fills spontaneously when its intrusion pressure is reached. Note that pores that have already filled with liquid are at the same pressure as the external liquid and thus do not undergo further compression. Thus, the resulting model is one wherein pores initially deform under applied pressure until the pressure is reached at which they spontaneously fill by capillary intrusion; once filled, these pores do not undergo any further elastic deformation.

Upon compression, a membrane that deforms elastically and isotropically does so according to the following equation:

$$dP = -K(dV/V) \quad (11)$$

from which one obtains

$$V_e = V_0 \exp(-P/K) \quad (12)$$

where  $V_0$  is the original volume of the pore.

Importantly, there exists a critical pore size below which elastic compression of the pore decreases its diameter faster than its intrusion pressure is approached. Such pores never fill by capillary intrusion. That this is the case can be seen by

plotting as a function of pressure the diameter of a pore with initial diameter  $D_0$  and the intrusion diameter  $D_i$  according to Eq. (1). For  $D_0 < D_{0,c}$ , the curves do not intersect, which indicates that such pores never realize the pressure required to fill them by capillary intrusion.  $D_{0,c}$  and the critical pressure  $P_c$  above which intrusion ceases to occur are identified with the  $D_0$  curve that lies tangent to Eq. (1). To find this, we equate the elastic compression diameter  $D_e$  with the intrusion diameter  $D_i$ , as well as their first derivatives with respect to pressure. For this purpose, we must first rewrite Eq. (12) in terms of diameter. If the pores have volume  $V = \pi D^2 l / 4$ , we obtain:

$$D_e = D_0 \exp(-P/nK) \quad (13)$$

where  $2 \leq n \leq 3$  is the dimensionality of elastic deformation: for pores that deform such that  $l$  remains constant,  $n=2$ , whereas for pores that deform such that the aspect ratio  $l/D$  of the pore remains constant,  $n=3$ . In the analysis that follows, we have used  $n=3$ .

Next, equating  $D_i$  and  $D_e$  and their first derivatives with respect to pressure, and solving for  $P_c$  and  $D_{0,c}$ , we obtain:

$$P_c = nK \quad (14)$$

$$D_{0,c} = \alpha e^{1/nK} \quad (15)$$

Now, for a single pore of volume  $V_0$ , one can write:

$$v(P) = V_0 \left[ \int_0^P K^{-1} \exp(-P'/K) dP' + \int_0^P \exp(-P'/K) \delta(P' - P^*) dP' \right] \quad (16)$$

The first term represents the volume of liquid measured as the membrane deforms elastically. As in the case of buckling, this volume is not subject to the same error associated with intrusion into a pore of geometry C in Fig 1a, since the pore deforms affinely. In contrast to buckling, elastic deformation should also be reversible and not give rise to hysteresis during a pressurization/depressurization cycle. The second term represents the volume of liquid that actually intrudes into the (deformed) pore, so long as  $P^* = P_i < P_c$ .

For a distribution of pores such as that described by Eq. (6), it is necessary to realize that  $V_0$  becomes a function of pressure, as the largest pores are

sequentially filled with liquid. In the study of aerogels, an empirical power law for modulus as a function of extent of compression during porosimetry was invoked [6]. Interestingly, it was subsequently proposed that the power law relation between modulus and density in such aerogels may be explained as a consequence of the buckling behavior described above [13]. In our model, the increasing effective stiffness of the material is solely a consequence of intrusion of liquid into some fraction of the pores of the material, which is accounted for by the reduction in unfilled, compressible pore volume with increasing pressure. By equating  $D_i$  from Eq. (1) with  $D_e$  from Eq. (13), we obtain an equation for the original diameter of pores that are filled by intrusion at a given pressure, valid up to  $P=P_c$ :

$$D_0(P) = \begin{cases} \frac{\alpha}{P} \exp\left(\frac{-P}{nK}\right) & P < P_c \\ D_{0,c} & P \geq P_c \end{cases} \quad (17)$$

All pores smaller than  $D_0(P)$  remain unfilled at pressure  $P$ . Thus, we define the original volume of pores that remain unfilled up to a pressure  $P$ :

$$V_{unf}(P) = \int_0^{D_0(P)} \rho(D') \mathcal{V}(D') dD' \quad (18)$$

For the cumulative volume of liquid measured during the liquid intrusion experiment, we write:

$$v(P) = \int_0^P V_{unf}(P') K^{-1} \exp(-P'/K) dP' + \int_0^P \rho(D_0) \mathcal{V}(D_0) \left[ -\frac{dD_0}{dP'} \right] \exp(-P'/K) \delta(P' - P^*) dP' \quad (19)$$

where

$$-\frac{dD_0}{dP} = D_0 \left( \frac{1}{nK} - \frac{1}{P} \right) \quad (20)$$

from Eq. (17), and in the second term  $P^* \leq P_c$ . Finally, the log differential volume measured as a function of  $P$  becomes:

$$\frac{dv(P)}{d \log P} = V_{unf}(P) \frac{P}{K} \exp\left(-\frac{P}{K}\right) + \rho(D_0) V\left(D_0 \left[-\frac{dD_0}{dP}\right]\right) P \exp\left(-\frac{P}{K}\right) \quad (21)$$

Measurements of  $v(P)$  and  $dv(P)/d \log P$  are readily available from liquid intrusion experiments. Analysis of these data using Eq. (7) and Eq. (9), for the buckling-intrusion case, or Eq. (19) and Eq. (21), for the elastic compression-intrusion case, allows us to determine the relative importance of the two deformation mechanisms and to quantify correctly the pore volume (or size) distribution in the presence of deformation.

### **Solution method**

The liquid intrusion experiment generates data for the cumulative volume of liquid that enters the sample cell as a function of pressure. Since it cannot distinguish whether the liquid intrudes into pores of the sample or replaces volume of the sample lost through deformation, it is desirable to correct the data for possible buckling and/or elastic compression before interpreting the results in terms of a pore volume distribution or a pore size distribution. This is readily done using the theory outlined above. Given a set of data for  $v(P)$  versus  $P$ , the goal is to solve for the joint function  $\rho(D)V(D)$ , which corresponds to the pore volume distribution; if the function  $V(D)$  is known explicitly, one can further solve for the pore size distribution  $\rho(D)$ . It is convenient to formulate the problem generically as a set of linear equations:

$$A(P, D) [\rho(D)V(D)] - dv(P)/d \log P = 0 \quad (22)$$

where the matrix  $A(P, D)$  is obtained from Eq. (9) or Eq. (21) for the cases of buckling-intrusion transition or elastic compression with intrusion, respectively. The vector  $dv(P)/d \log P$  is easily obtained from  $v(P)$  vs  $P$  by numerical differentiation using 2-point or 3-point formulas.

For the buckling-intrusion transition,  $A(P, D)$  is diagonal, since the volume associated with a pore of size  $D$  is measured entirely at a pressure  $P$ , dependent only on whether the mechanism is one of buckling or intrusion. The solution is straightforward:

$$[\rho(D)V(D)] = \frac{[dv(P)/d \log P]_{\text{expt}}}{[-dD/dP]P} \quad (23)$$

where  $[-dD/dP]$  is obtained from Eq. (8) and  $D$  is obtained from Eq. (1) or Eq. (2) for  $P > P_c$  (intrusion) and  $P < P_c$  (buckling), respectively.

For the case of intrusion accompanied by elastic compression, we encounter the problem that the equation for isotropic compression does not permit us to distinguish pores of one size from another. Thus, only for pressures less than  $P_c$ , where liquid actually intrudes into pores, can the corresponding pore size distribution be determined. Thus, for soft materials in the presence of elastic deformation, there is an intrinsic limitation to the liquid intrusion experiment: the distribution of pores smaller than  $D_{0,c}$  (Eq. 15) cannot be characterized. Nevertheless, the distribution of pores larger than  $D_{0,c}$  can still be extracted. First, we limit the values of  $P$  for which Eq. (22) is solved to those where  $P < P_c$ , according to Eq. (14). Next, we expand Eq. (18) numerically in terms of  $\rho(D_0)$ :

$$\int_0^{D_0(P)} \rho(D') V(D') dD' \cong \frac{1}{2} \rho(D_{0,c}) V(D_{0,c}) (D_{0,c} - D_{0,j=2}) + \frac{1}{2} \sum_{j=2}^{n-1} \rho(D_{0,j}) V(D_{0,j}) (D_{0,j+1} - D_{0,j-1}) + \frac{1}{2} \rho(D_0(P)) V(D_0(P)) (D_0(P) - D_{0,j=n-1}) \quad (24)$$

where the integration runs from  $D_{0,c}$  to  $D_0(P)$  in  $n-1$  intervals. Finally, we construct the matrix  $A(P,D)$  as follows:

$$\begin{aligned} A_{ii}(P_i, D_i) &= \frac{1}{2}(D_{0,i} - D_{0,i+1}) \\ &\quad + [dD_0/dP] P_i \exp(-P_i/K) \\ A_{i,i < j < n}(P_i, D_j) &= \frac{1}{2}(D_{0,j+1} - D_{0,j-1}) \\ A_{i,n}(P_i, D_n) &= \frac{1}{2}(D_{0,n} - D_{0,n-1}) \end{aligned} \quad (25)$$

The resulting  $A$  matrix is upper triangular and can be solved by back substitution to obtain  $\rho(D_0)V(D_0)$ .

## RESULTS AND DISCUSSION

### Model System

In this section, we explore the consequences of both deformation modes for a model system, in order to recognize their signature features. We first consider the case for the buckling-intrusion transition. For purposes of illustration, we assume a membrane with Young's modulus  $E=100$  MPa, and Poisson's ratio  $\nu=0.3$ . For the shell thickness,  $t$ , a value equal to the fiber diameter seems the most reasonable approximation. These values are chosen primarily for illustrative purposes, but are believed to be representative of electrospun nonwoven mats. For mercury, with  $\theta=140^\circ$  and  $\gamma=0.48$  N/m,  $\alpha=1.47$  N/m. All volumes are normalized to a total pore volume of 1.0, so the characteristic length  $l$  is fixed for a given pore size distribution, according to:

$$\frac{V_{total}}{l} = \frac{4}{\pi} \int_0^\infty \rho(D) D^2 dD \quad (26)$$

Fig. 2 illustrates the crossover from buckling to intrusion at the critical pressure for four different shell thicknesses or fiber diameters:  $t=20$   $\mu\text{m}$ , 2  $\mu\text{m}$ , 1.2  $\mu\text{m}$  and 0.2  $\mu\text{m}$ . As the fiber diameter decreases, buckling of the cylindrical pore persists to higher pressures.

To illustrate the effects of shell thickness, or fiber diameter, on liquid volume measurements, we consider a prototypical log normal pore size distribution given by Eq. (27) and shown in Fig. 3:

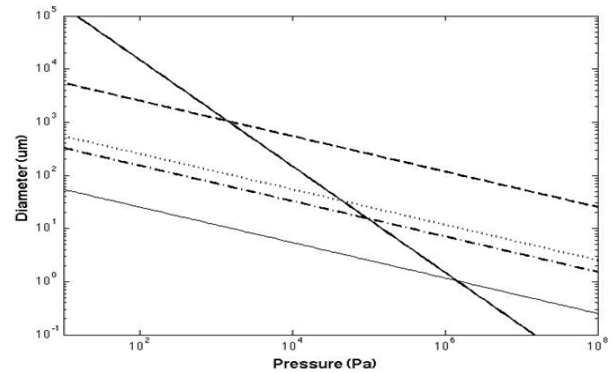


FIGURE 2. Pore diameter vs pressure scaling for liquid intrusion according to eq (1) (thick solid line) and for buckling of cylindrical shells according to eq 2 for four shell thicknesses:  $t=20$   $\mu\text{m}$  (dashed line); 2  $\mu\text{m}$  (dotted line); 1.2  $\mu\text{m}$  (dash-dot line); 0.2  $\mu\text{m}$  (thin solid line). The corresponding transition pressures  $P_c$  are: 1.38, 44.9, 96.0 and 718 kPa, respectively. The transition diameters are: 1043, 33.0, 15.3 and 1.0  $\mu\text{m}$ , respectively.

$$\rho(D) = \frac{1}{D\sigma\sqrt{2\pi}} \exp\left[-\left(\frac{\log D - \mu}{2\sigma}\right)^2\right] \quad (27)$$

with  $\mu=\log(12)$  and  $\sigma=0.5$ . Fig 4(a) shows the cumulative volume distribution  $v(P)$  given by Eq. (7) and Eq. (8), for the same four fiber diameters. For the given mechanical properties of the mat, the largest fibers (20  $\mu\text{m}$  diameter) exhibit a transition from buckling to liquid intrusion around  $D_c=1043$   $\mu\text{m}$ , which is in the high end tail of the pore size distribution; for these fibers, essentially all of the liquid volume is measured during intrusion. For the 2  $\mu\text{m}$  and 1.2  $\mu\text{m}$  fibers, the transition occurs around  $D_c=33$  and 15.3  $\mu\text{m}$ , respectively, well within the important range of pore sizes. Both curves exhibit a low pressure tail that is less steep than the intrusion curve, indicative of the buckling phenomenon. The smallest fibers (0.2  $\mu\text{m}$ ) transition around  $D_c=1.0$   $\mu\text{m}$ , which is below the relevant pore size range; essentially all of the liquid volume is measured during buckling in this case. Applying Eq. (1) to this data would yield a gross overestimate of the true pore size distribution. That this is the case can be clearly seen by converting the volume data into a log differential intrusion volume vs equivalent capillary diameter, according to Eq. (10); the results of this are shown in Fig 4(b). The pore size distribution is correctly described only for the largest, 20  $\mu\text{m}$  fibers. The 2  $\mu\text{m}$  fibers show a sharp peak at the correct diameter, but a long tail on the high end of the distribution. The 1.2  $\mu\text{m}$  fibers apparently show a bimodal pore size distribution, with the maximum actually due to the buckling-intrusion transition itself;

neither peak corresponds to the true peak of the pore size distribution.

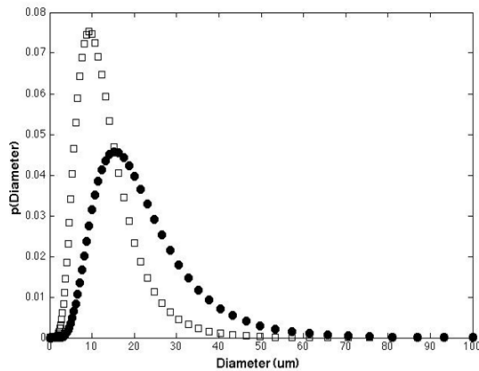


FIGURE 3. A prototypical log normal pore size distribution,  $p(D)$  (squares). Also shown is the pore volume distribution (filled circles). Note that the pore volume distribution is necessarily shifted toward larger diameter.

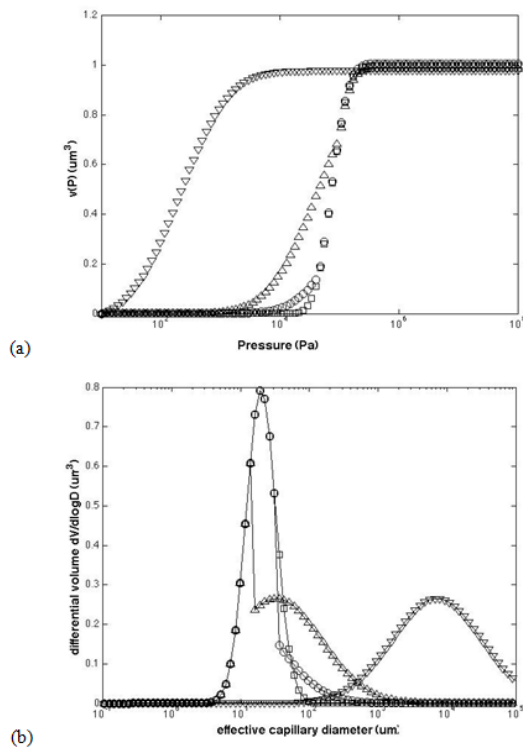


FIGURE 4. (a) cumulative volume  $v(P)$  versus pressure. (b) log differential volume  $dV/d\log D$  versus equivalent capillary diameter, usually assumed during a liquid intrusion experiment. In both plots, 20  $\mu\text{m}$  fibers (squares), 2  $\mu\text{m}$  fibers (circles), 1.2  $\mu\text{m}$  fibers (triangles) and 0.2  $\mu\text{m}$  fibers (inverted triangles).

Finally, the smallest 0.2  $\mu\text{m}$  fibers show an artificially broadened pore size distribution that is furthermore shifted upward in pore size by almost

three orders of magnitude. These cases demonstrate just how critical it is to account for buckling of pores during liquid intrusion measurements when it occurs.

Next, we consider the case in which elastic compression accompanies intrusion. *Fig 5* shows the results of the preceding example for  $E=100$  MPa and also for  $E=0.1$  MPa. In the case of higher modulus, the cumulative volume versus pressure profile is imperceptibly different from the intrusion profile. The critical diameter  $D_c$  below which intrusion does not occur is 0.016  $\mu\text{m}$ , too low to affect the measurement noticeably. However, upon reduction of modulus by three orders of magnitude, the effect of elastic compression becomes significant. As in the case of buckling, the cumulative volume curve exhibits a low pressure tail that is considerably extended relative to that associated with intrusion alone. The total cumulative volume is also measurably less, since  $D_c$  increases to 16  $\mu\text{m}$ , and a significant fraction of the pores never undergo intrusion. Also shown in *Fig 5a* are the individual contributions to cumulative volume  $v(P)$  associated with compression of the mat and with intrusion into the pores of the mat, respectively. It is apparent that elastic compression begins at much lower pressures than intrusion, and ultimately accounts for 75% of the total liquid volume measured in this example. *Fig. 5b* shows the differential volume versus equivalent capillary diameter curve for both  $E=100$  MPa and for  $E=0.1$  MPa. While the higher modulus membrane provides a faithful measure of the true pore size distribution, the lower modulus membrane is shifted to larger pore diameter and exhibits a high pore diameter tail. The peak shift in this case is relatively modest. From these results, we conclude that for the range of fiber sizes and pore sizes typical of electrospun nonwoven membranes, buckling is likely to be more important than elastic compression, since it gives the larger effect for materials in the relevant range of Young's modulus.

### Experimental System

Analysis is reported here for three electrospun nonwoven samples of poly( $\epsilon$ -caprolactone) (PCL) fibers with average fiber diameters that vary over an order of magnitude. The apparatus and methods used for the production of these samples were the same as reported previously [14,15]. The solution and process conditions for each sample are summarized in *Table 1*. Representative SEM images (JSM-6060, JEOL Ltd, Tokyo, Japan) of the three samples are shown in *Fig 6*. The corresponding fiber sizes, determined from the SEM micrographs by measuring diameters

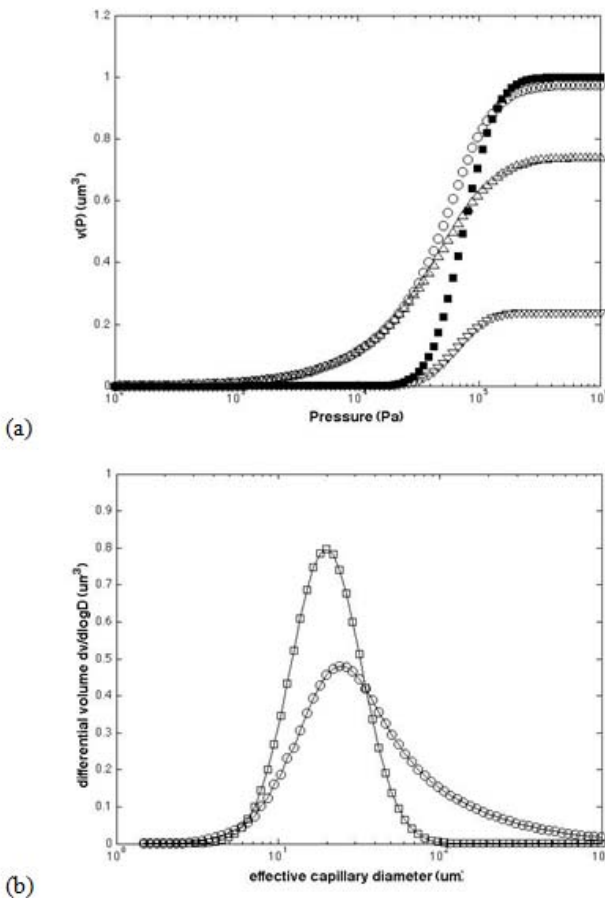


FIGURE 5. (a) cumulative volume versus pressure.  $E=100$  MPa (filled squares).  $E=0.1$  MPa (circles); partial volume measured due to intrusion (inverted triangles); partial volume measured due to elastic compression (triangles). (b) log differential volume  $dV/d\log D$  versus equivalent capillary diameter for  $E=100$  MPa (squares) and for  $E=0.1$  MPa (circles).

of 40 to 60 fibers from both sides of the sample using the *analySIS v3.2* software (Software Imaging Systems, Münster, Germany), are  $2.49 \pm 0.82$ ,  $6.50 \pm 0.57$  and  $18.0 \pm 1.9$   $\mu\text{m}$ . Mercury porosimetry was performed using an Autopore IV porosimeter (Micromeritics, Norcross, GA).

Rectangular samples approximately 1 cm x 2 cm in dimension were inserted into the penetrometer, and

care was taken to ensure that the entire sample surface was accessible to the mercury. The penetrometer was filled initially at 3500 Pa, and the threshold for equilibrium intrusion rate was set to 0.03  $\mu\text{l/g/s}$  to ensure equilibration at each pressure. Information regarding each sample and results of the analysis are provided in *Table 2*. *Fig. 7* shows the typical result of mercury porosimetry for the 6.50  $\mu\text{m}$  fiber sample. From the total volume of mercury measured during the experiment, a sample porosity of 0.83 was determined. This value is in good agreement with a porosity of 0.82 determined gravimetrically from the area density of the sample, the thickness of the mat and a PCL density of 1.145  $\text{g/cm}^3$ , corresponding to 40% crystallinity.

Qualitatively similar porosimetry data have been reported for other electrospun materials [3,4] and for xerogels [8,16]. Each of these cases are characterized by an abrupt change in slope of  $v(P)$  versus  $P$  in the raw porosimetry data, which is indicative of the transition from buckling to intrusion. In *Fig 7* this occurs around  $P_c=4.8 \times 10^4$  Pa. To confirm that this pressure corresponds to a transition from sample deformation to liquid intrusion, we performed a second series of experiments in which this sample was pressurized in the porosimeter to an intermediate pressure and then depressurized, after which the sample was reweighed. For intermediate pressures less than  $5 \times 10^4$  Pa, the sample weight after the pressurization/depressurization cycle was essentially unchanged from the original weight. We also observed considerable hysteresis in the  $v(P)$  vs  $P$  curve for pressurization-depressurization cycle at intermediate pressures less than  $5 \times 10^4$  Pa. Taken together, these two observations indicate that the volume of mercury measured below  $5 \times 10^4$  Pa corresponds predominantly to an irreversible process that does not involve intrusion of mercury, i.e. buckling deformation. For intermediate pressures greater than  $5 \times 10^4$  Pa, the sample weight increases dramatically with increasing pressure, indicative of mercury intrusion into the sample at higher pressure. Hysteresis was again observed, but it was not as significant as at the lower pressures.

TABLE I: Solution and Process Conditions

|   | Sample #1 | Sample #2 | Sample #3 |
|---|-----------|-----------|-----------|
| PCL solute (w/w)  | 11%       | 20%       | 15%       |
| Solvent composition (CHCl <sub>3</sub> :CH <sub>3</sub> OH) | 3:1       | 3:1       | 1:0       |
| Flow rate (ml/min)  | 0.1       | 0.1       | 0.2       |
| Applied voltage (kV)  | 32.8      | 37.8      | 37.5      |
| Spin distance (cm)  | 40        | 42        | 55        |

TABLE II: Results for Electrospun Poly( $\epsilon$ -caprolactone) Nonwoven Membranes

|  | Sample #1         | Sample #2         | Sample #3         |
|--|-------------------|-------------------|-------------------|
| Fiber diameter ( $\mu\text{m}$ )                         | 2.49 $\pm$ 0.82   | 6.50 $\pm$ 0.57   | 18.0 $\pm$ 1.9    |
| Area density (g/cm <sup>2</sup> )                        | 0.01289           | 0.01938           | 0.00676           |
| Thickness (mm)   | 0.852 $\pm$ 0.038 | 1.004 $\pm$ 0.041 | 0.700 $\pm$ 0.040 |
| Hg volume (ml/g)   | 5.04              | 4.50              | 5.05              |
| Porosity (porosimetry)                                   | 0.842             | 0.834             | 0.843             |
| Porosity (gravimetric)                                   | 0.857             | 0.818             | 0.828             |
| $P_c$ (kPa) <sup>(a)</sup>                               | 170               | 48                | 17                |
| $D_c$ ( $\mu\text{m}$ ) <sup>(b)</sup>                   | 8.5               | 30                | 85                |
| $E_{eff}$ (MPa) <sup>(c)</sup>                           | 3.5               | 2.5               | 0.9               |
| $E$ (MPa) <sup>(d)</sup>                                 | 15.1 $\pm$ 1.2    | 10.2 $\pm$ 0.6    | 17.1 $\pm$ 1.3    |
| Vol. ave. pore diameter ( $\mu\text{m}$ ) <sup>(e)</sup> | 12 $\pm$ 6.7      | 27 $\pm$ 13       | 78 $\pm$ 26       |
| Area ave. pore diameter ( $\mu\text{m}$ ) <sup>(f)</sup> | 7.9 $\pm$ 5.8     | 20 $\pm$ 12       | 65 $\pm$ 29       |
| Size ave. pore diameter ( $\mu\text{m}$ ) <sup>(g)</sup> | 5.3 $\pm$ 3.7     | 5.0 $\pm$ 8.6     | 50 $\pm$ 27       |

(a) applied pressure at buckling/intrusion transition; (b) pore diameter at buckling/intrusion transition; (c) effective sample modulus, determined from buckling/intrusion transition; (d) sample modulus from tensile measurement; (e) average pore diameter and standard deviation, from pore volume distribution; (f) average pore diameter and standard deviation, from pore area distribution. For pores comprised of cylindrical sections, this average is equal to  $4V/S$ , where  $V$  is the total pore volume and  $S$  is the total pore area; (g) average pore diameter and standard deviation, from pore size distribution.

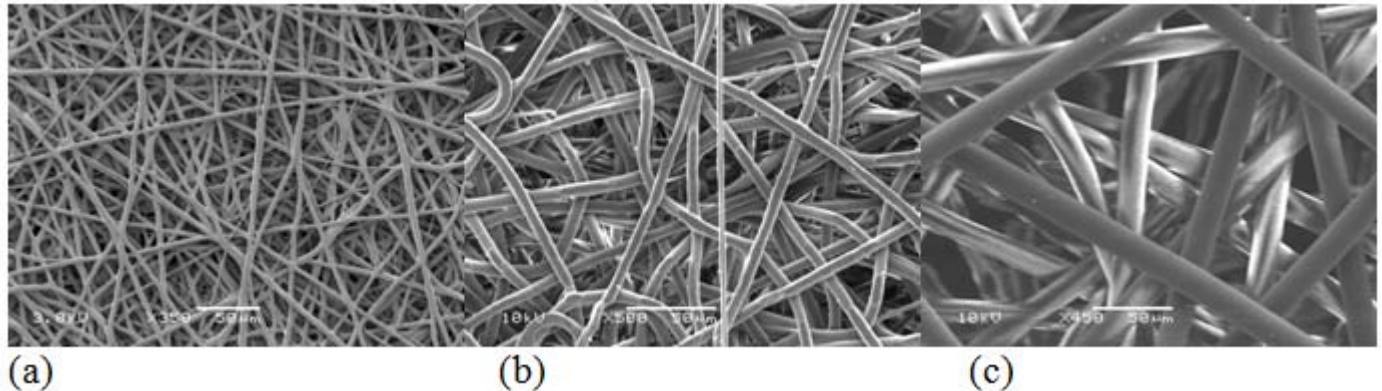


FIGURE 6. Scanning electron micrographs of PCL nonwoven fiber samples. (a) Sample #1 ( $t=2.49 \mu\text{m}$ ); (b) Sample #2 ( $t=6.50 \mu\text{m}$ ); (c) Sample #3 ( $t=18.0 \mu\text{m}$ ). All scale bars are  $50 \mu\text{m}$ .

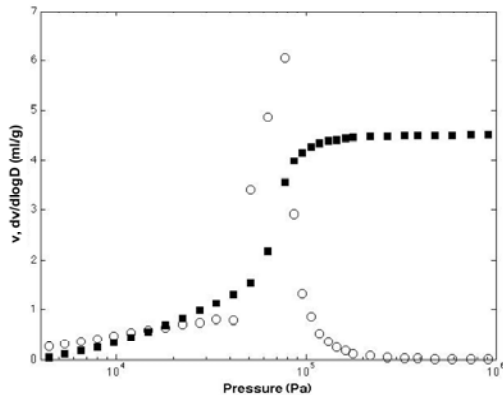


FIGURE 7. Mercury porosimetry results for a typical electrospun nonwoven mat. PCL fibers, average fiber diameter: 6.50  $\mu\text{m}$ . Raw data for mercury volume  $v(P)$  versus the logarithm of pressure  $\log P$  (filled black squares); log differential intrusion volume  $dv(P)/d\log P$  vs  $\log P$ : (open circles).

Using this experimentally observed value of  $P_c$  and the average fiber diameter of 6.50  $\mu\text{m}$  from SEM, we can estimate via Eq. (4) the effective elastic modulus,  $E_{eff}$ , of the mat to be 2.5 MPa. Similar analysis for the other two samples yields  $E_{eff}$  equal to 3.5 MPa and 0.9 MPa for the samples having fiber diameters of 2.49 and 18.0  $\mu\text{m}$ , respectively. These values of  $E_{eff}$  are about 1/4 of the elastic moduli,  $E$ , measured for the same nonwoven mats under tensile deformation (Zwick, 3-5 cm sample gauge length, 0.001  $\text{s}^{-1}$  strain rate). However, they are comparable to the moduli reported previously by others for nonwoven mats of electrospun PCL fibers in the diameter range 200-700 nm [17,18]. The quantitative discrepancies between  $E_{eff}$  and  $E$  are likely due to the simplicity of the buckling model and our assumption that the shell thickness  $t$  is equal to the average fiber diameter.

Fig 8 shows the pore volume distribution  $\rho(D)V(D)$  obtained for the 6.50  $\mu\text{m}$  fiber sample using Eq. 23 for the buckling-intrusion transition. The average and standard deviation of the distribution is  $27 \pm 13$   $\mu\text{m}$ . Assuming the pores are comprised of segments with volume  $V(D) \sim D^2$ , we obtain a pore size distribution with average and standard deviation of  $5.0 \pm 8.6$   $\mu\text{m}$  for this sample, indicative of a highly skewed distribution. We find that the determination of pore size distribution in our data is subject to substantial noise in the count of pores below 5  $\mu\text{m}$ , due to the small sample sizes used; these in turn were limited by the size of the penetrometer bulb available for this work. For this reason, the pore size distribution tends to exhibit multiple peaks and is believed to be less accurate than the pore volume

distribution here. Results for the other two samples are provided in Table 2.

From these results, it is evident that the average diameter of a pore increases in proportion to fiber size, in accord with the relatively small variation in overall porosity between samples. Also shown in Fig 8 is the pore volume distribution plotted versus the equivalent capillary diameter, i.e. the distribution obtained if one assumes that no buckling occurs. The latter suggests that there is a discontinuity in the pore volume distribution around  $D=30$   $\mu\text{m}$  and that there exists a broad tail in the distribution that persists up to pores having diameters 100-300  $\mu\text{m}$ ; upon correction for deformation, both of these features are determined to be spurious. The large diameter pores, in particular, are inconsistent with SEM observations (c.f. Fig. 6). Analysis of the porosimetry data using the elastic compression-intrusion model with a Young's modulus on the order of 1 MPa indicates that elastic compression has little effect on the measured pore volume distribution for this sample.

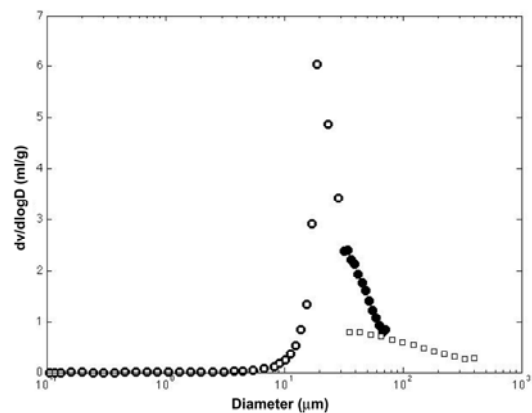


FIGURE 8. Pore volume distribution for a PCL mat with average fiber diameter of 6.50  $\mu\text{m}$ . Data corrected for buckling/intrusion transition (filled circles); Uncorrected results assuming applicability of the Washburn equation over the entire pressure range (open squares).

## CONCLUSIONS

A theory for the determination of pore diameter distributions by liquid intrusion porosimetry in the presence of radial buckling of the pores or elastic compression of the sample has been presented here. The theory is developed with the specific case of nonwoven fibrous media in mind, but is otherwise quite general, and can be incorporated as part of any analysis of porous media by liquid intrusion porosimetry. We find that irreversible buckling of the

pores is likely to be more important than the reversible elastic compression of the electrospun fiber mat during the typical mercury porosimetry experiment.

These results indicate that deformation of the sample must be taken into consideration when determining the pore diameter distribution of fibrous mats comprised of small diameter (<10  $\mu\text{m}$ ) polymer fibers. Failure to do so can lead to erroneous conclusions regarding pore diameters and their dependence on sample preparation conditions. This is especially critical at the present time, when electrospinning is being widely used to produce nonwoven fiber mats with fiber diameters below 10  $\mu\text{m}$ , and to modify their pore size distribution [19-22]. Recent attempts to characterize the porosity or pore size distribution of such materials may merit reconsideration in light of these results [3,4,23-25].

#### ACKNOWLEDGMENTS

We gratefully acknowledge partial funding for this work through the Nicolas G. and Dorothea K. Dumbros Scholarship and Fellowship Fund (JLL) and from the U.S. Army through the Institute for Soldier Nanotechnologies (ISN), under contract DAAD-19-02-D-0002 with the U.S. Army Research Office. We also wish to thank Dr. S. Norris for informative discussion regarding the theoretical analysis for elastic compression.

#### REFERENCES

- [1] Jena, A., Gupta, K., *Int. Nonwovens J.*, 45, Fall 2003.
- [2] Jena, A., Gupta, K., *Int. Nonwovens J.*, 25, Summer 2005.
- [3] Ryu, Y.J., Kim, H.Y., Lee, K.H., Park, H.C., Lee, D.R., *Eur. Polym. J.*, 39, 1883, 2003.
- [4] Ko, J.B., Lee, S.W., Kim, D.E., Kim, Y.U., Li, G., Lee, S.G., Chang, T.S., Kim, D., Joo, Y.L., *J. Porous Mater.*, 325, 2006.
- [5] Li, D.P., Frey, M.W., Joo, Y.L., *J. Membrane Sci.*, 286 (1-2), 104, 2006.
- [6] Scherer, G.W., Smith, D.M., Stein, D., *J. Non-Cryst. Solids*, 186, 309, 1995.
- [7] Pirard, R., Blacher, S., Brouers, F., Pirard, J.P., *J. Mater. Res.*, 10, 2114, 1995.
- [8] Pirard, R., Heinrichs, B., Van Cantfort, O., Pirard, J.P., *J. Sol-Gel Sci. Technol.*, 13, 335, 1998.
- [9] Moro, F., Böhni, H., *J. Coll. Int. Sci.*, 246, 135, 2002.
- [10] Brush, D.O., Almroth, B.O., *Buckling of Bars, Plates and Shells*, McGraw-Hill: New York, 1975.
- [11] Flügge, W., *Stresses in Shells*, 2<sup>nd</sup> Ed., Springer-Verlag: New York, 1973.
- [12] Gibson, L.J., Ashby, M.F., *Proc. Roy. Soc. Lond. A*, 382, 43, 1982.
- [13] Pirard, R., Pirard, J.P., *J. Non-Cryst. Sol.*, 212,262, 1997.
- [14] Shin, Y. M.,Hohman, M. M., Brenner, M. P., Rutledge, G.C., *Polymer*, 42, 9955, 2001.
- [15] Fridrikh, S. V., Yu, J. H., Brenner, M. P., Rutledge, G. C., *Phys. Rev. Lett*, 90, 144502, 2003.
- [16] Alié, C., Pirard, R., Pirard, J.P., *Coll. Surf. A*, 187, 367, 2001.
- [17] Bölgen, N., Menciloglu, Y.Z., Acatay, K., Vargel, I., Piskin, E., *J. Biomater. Sci. Polym. Ed.*, 16(12), 1537, 2005.
- [18] Thomas, V., Jose, M.V., Chowdury, S., Sullivan, J.F., Dean, D.R., Vohra, Y., *J. Biomater. Sci. Polymer Edn*, , 17(9), 969, 2006.
- [19] Lee, Y.H., Lee J.H., An, I.-G., Kim, C., Lee, D.S, Lee, Y.K, Nam, J.-D., *Biomaterials*, 26, 3165, 2005.
- [20] Mitchell, S.B. Sanders, J.B., *J. Biomed. Mater. Res. A*, 78, 110, 2006.
- [21] Simonet, M., Schneider, O.D., Neuenschwander, P., Stark, W.J, *Polym. Eng. Sci.*, 47, 2020, 2007.
- [22] Nam, J., Huang Y., Agarwal S., Lannutti, J., *Tissue Eng.*, 13, 2249, 2007.
- [23] Kwon, I.K., Kidoaki, S., Matsuda, T., *Biomaterials*, 26, 3929, 2005.

[24] Kidoaki, S., Kwon, I.K., Matsuda, T., *J. Biomed. Mater. Res. B*, 76, 219, 2006.

[25] Pham, Q.P., Sharma, U., Mikos, A.G., *Biomacromolecules*, 7, 2796, 2006.

#### **CORRESPONDING AUTHOR'S ADDRESS**

**G. C. Rutledge**

Massachusetts Institute of Technology  
Department of Chemical Engineering  
77 Massachusetts Avenue  
Room 66-550  
Cambridge, MA 02139  
UNITED STATES